Journal of Solid State Chemistry 183 (2010) 2558–2564

Contents lists available at ScienceDirect

Journal of Solid State Chemistry

journal homepage: www.elsevier.com/locate/jssc

Pressure-induced transition in Tl_2MoO_4

Denis Machon [a,*], Karen Friese [b], Tomasz Breczewski [c], Andrzej Grzechnik [b]

[a] Université de Lyon, F-69000, France – Univ. Lyon 1, Laboratoire PMCN, CNRS, UMR 5586, F-69622 Villeurbanne Cedex
[b] Departamento de Física de la Materia Condensada, Facultad de Ciencia y Tecnología, Universidad del País Vasco, Apartado 644, 48080 Bilbao, Spain
[c] Departamento de Física Aplicada II, Facultad de Ciencia y Tecnología, Universidad del País Vasco, Apartado 644, 48080 Bilbao, Spain

ARTICLE INFO

Article history:
Received 21 May 2010
Received in revised form
19 August 2010
Accepted 30 August 2010
Available online 16 September 2010

Keywords:
High-pressure
Molybdates
Raman spectroscopy
X-ray diffraction
Optical absorption

ABSTRACT

Tl_2MoO_4 has been studied under high-pressure by X-ray diffraction, Raman spectroscopy, and optical absorption measurements. A first-order phase transition is observed at 3.5 ± 0.5 GPa. The nature (ordered vs. disordered) of the high-pressure phase strongly depends on the local hydrostatic conditions. Optical absorption measurements tend to show that this transition is concomitant with an electronic structure transformation. Prior to the transition, single crystal X-ray diffraction shows that pressure induces interactions between MoO_4 fragments and the Mo coordination number tends to increase. In addition, the stereoactivity of the lone-pair electrons on the three symmetrically independent Tl-sites is not uniform; while for two sites the stereoactivity decreases with increasing pressures for the third site the stereoactivity increases.

1. Introduction

In compounds containing isolated polyhedra, pressure leads to a reduction of space between them until a significant interaction may be induced. In such a case, the compound has to adapt both structurally (the presence of highly symmetrical polyhedra imposes strong local symmetry constraints) and thermodynamically (taking into account new chemical interactions). This could lead to stabilize an amorphous state that appears as a good compromise. Such pressure-induced transitions have been observed in rare-earth molybdates $RE_2(MoO_4)_3$ (with RE=rare earths such as Gd, Eu, Tb, Nd). Using a combination of experimental and simulation techniques, it has been shown that at a certain pressure, the interactions between MoO_4 tetrahedra in $Eu_2(MoO_4)_3$ induces a transformation from a system of weakly interacting MoO_4 fragments to a system of weakly interacting Mo atoms embedded in a fully p-hybridized oxygen gas accompanied with a crystal-to-amorphous transition [1].

The aim of this study is to investigate the possible extension of this model to different structures and chemical compositions but keeping the isolated MoO_4 tetrahedra as one of the basic building units in the structures.

Tl_2MoO_4 is a perfect candidate for such study. This compound has first been studied by Gaultier and Pannetier [2] who described three temperature-induced phase transitions at 776, 673 and 311 K. However, only the structures of the two lowest temperature polymorphs have been characterized in detail. The polymorph of Tl_2MoO_4, which is stable above 311 K, crystallizes in space group $P\bar{3}m1$ (Z=2) and is isostructural to the glaserite structure [3]. The corresponding crystals have a light yellow colour. In this phase, Mo is in tetrahedral coordination, and, as required for this study, the MoO_4-tetrahedra are isolated with respect to each other. They are, however, connected via three different coordination polyhedra, which form around the three symmetrically independent monovalent Tl^+ cations. The coordination around Tl1 can be described as a distorted octahedron. Each of the corners of the octahedron shares one oxygen atom with a neighbouring MoO_4-tetrahedron. Tl2 has a coordination number of 6+6. The corresponding polyhedron can be described as a trigonal antiprism with 6 additional meridional anions in a hexagonal outline. They share common edges with MoO_4-tetrahedra. Tl3 is coordinated by 10 oxygen atoms. Six of the oxygen atoms form a distorted meridional hexagon, while the other three oxygen atoms above it form the basis of a MoO_4 tetrahedron and the one oxygen below it forms the apex of another MoO_4 tetrahedron.

The polymorph of Tl_2MoO_4 below 311 K is monoclinic and acentric ($C2$, Z=4) [4]. At the phase transition $P\bar{3}m1 \rightarrow C2$, the MoO_4 tetrahedra are rotated leading to drastic changes in the coordination polyhedra of the Tl atoms and in the connection pattern between the Tl-polyhedra and the MoO_4 tetrahedra. The $Tl1O_6$ octahedra are strongly distorted in the monoclinic phase, while the coordination number for Tl2 and Tl3 decrease in the

* Corresponding author at: Laboratoire de Physique de la Matière Condensée et Nanostructures, Université Claude Bernard Lyon 1 et CNRS, UMR 5586, Domaine Scientifique de la Doua, Bâtiment Léon Brillouin, 43 Boulevard du 11 Novembre 1918, F 69622 Villeurbanne, France. Fax: +33 04 72 43 26 48.
E-mail address: denis.machon@univ-lyon1.fr (D. Machon).

0022-4596/$ - see front matter © 2010 Elsevier Inc. All rights reserved.
doi:10.1016/j.jssc.2010.08.036

Table 1
Group-theoretical analysis of the vibrational modes of $(MoO_4)^{2-}$ ions in the Tl_2MoO_4 structure (space group $C2$) at ambient conditions.

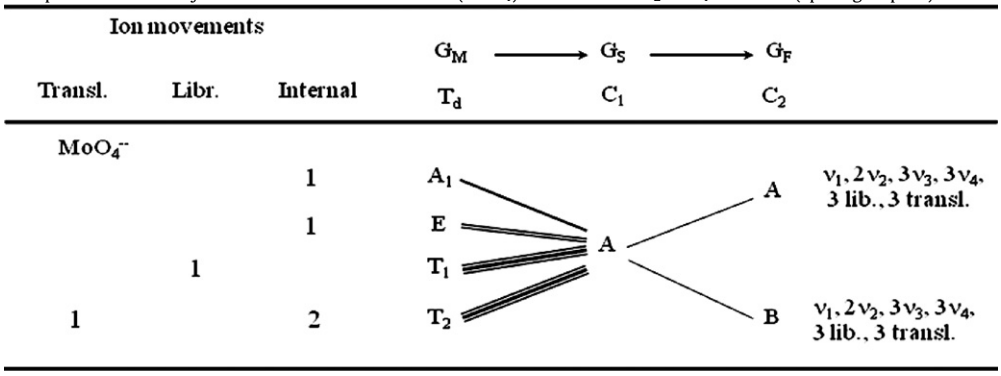

phase transition (Tl2: 12→10; Tl3: 10→9). The distortion of the MoO_4 tetrahedra is also increasing significantly at the phase transition and individual Mo–O distances are lengthened in the low symmetry polymorph. Part of the common edges between tetrahedra and Tl2–O polyhedra are changed to common corners and the common face between the Tl3–O polyhedra and the tetrahedral unit is changed to a common edge. The acentric monoclinic phase is affected by twinning and the crystals show relatively strong second harmonic generation signals ($d_{eff}=5.5\pm0.5$ pm V^{-1}; [4]).

To the best of our knowledge, the high pressure behaviour of Tl_2MoO_4 has not been studied up to now. As mentioned above, our main interest is focused on the influence of pressure on the interactions between the isolated tetrahedral units and the relationship to possible amorphization. However, another interesting aspect of this study is related to the fact that Tl^+ is a cation which has lone-electron pairs, whose stereoactivity might be substantially influenced by pressure. Stereoactivity of lone-pair electrons leads generally to strongly distorted coordination polyhedra, and is often related to the formation of acentric structures (like the low-temperature polymorph of Tl_2MoO_4), which in turn might be related to interesting optical properties (like e.g. second harmonic generation effects as observed in Tl_2MoO_4). The study of the high pressure behaviour of compounds containing lone-pair electrons might therefore lead to important impulses for the high-pressure synthesis of materials or might give indications to more "traditional" synthesis methods, making use of the concept of equivalence between hydrostatic and chemical pressure.

We studied the high-pressure behaviour of Tl_2MoO_4 at ambient temperature using single crystal diffraction in combination with Raman spectroscopy. In addition, we also carried out an accompanying optical absorption spectroscopy study to obtain details about the effect of hydrostatic pressure on the optical properties.

2. Experimental

The crystals of Tl_2MoO_4 were synthesized according to Ref. [3].

High-pressure Raman scattering experiments were carried out using a membrane diamond anvil cell with low-fluorescence diamonds having a culet size of 350 μm. The powdered sample was loaded into a hole drilled in a stainless steel gasket. Several ruby chips were distributed throughout the sample chamber, and the pressures were determined using the ruby fluorescence method. Raman spectra were obtained using a customized high-throughput optical system based on Kaiser optical filters and an Acton 300i spectrograph with sensitive CCD detection. Samples were excited using 514.5 nm radiation from an air-cooled Ar^+ laser. The beam was focused on the sample using a Mitutoyo 50× objective, with beam diameter ~2 μm at the sample. The scattered light was collected in backscattering geometry using the same lens. Optical absorption spectra were obtained on a limited spectral range using the same spectrometer and set-up as for the Raman experiments, and a white light source.

Single-crystal X-ray intensities to 7.33 GPa were measured from the crystal in the Ahsbahs-type diamond anvil cell [5] at room temperature using a STOE diffractometer IPDS-2T (Mo–$K\alpha$). A 250 μm hole was drilled into a stainless steel gasket preindented to a thickness of about 80 μm. The intensities were indexed, integrated, and corrected for absorption using the STOE software [6]. The areas of the images that were shaded by the diamond anvil cell were masked prior to integration. The intensities were integrated simultaneously with three orientation matrices, corresponding to the crystal of Tl_2MoO_4 and to the two diamonds of the cell. Due to their hemispherical shape, no absorption correction was necessary for the diamond anvils. The ruby luminescence method [7] was used for pressure calibration and a mixture of pentane and isopentane was used as pressure medium. All the data were processed and refined using the program JANA2006 [8].[1]

3. Results and discussion

3.1. Raman spectrum at ambient conditions

The Raman-active modes for Tl_2MoO_4 can be obtained using symmetry analysis (Table 1). Fourteen atoms located within the primitive unit cell corresponding to space group $C2$ (C_2^3) give rise to 39 ($\mathbf{k}=0$) zone-center vibrational modes. The ones predicted to be Raman active are

$$\Gamma_{raman} = 19A + 20B$$

The internal vibrations of the two tetrahedral $(MoO_4)^{2-}$ ions in the primitive cell are described in terms of in-phase (ν_1), and out-of-phase (ν_3) Mo–O stretching, and in two types of O–Mo–O bending modes (ν_2 and ν_4). These internal vibrations can couple in the crystal via the symmetry elements. The number of components and their symmetry are detailed in Table 1 using group-theoretical

[1] Further details of the crystallographic investigations can be obtained from the Fachinformationszentrum Karlsruhe, D-76344 Eggenstein-Leopoldshafen, Germany, on quoting the depository number CSD 421983.

analysis [9]. This table gives the correlation between the motions of anions in T_d symmetry and in the monoclinic symmetry C_2 through the site group C_1. For example, we expect the two ν_1 symmetric stretching vibrations to be distributed into A and B crystal modes. From this analysis, 18 internal modes are expected to be observed in the Raman spectra. Fig. 1 clearly shows that the actual number of observed bands is lower. Only eight vibrational modes can be clearly identified. This indicates that the molybdate ions interact weakly with the remaining structural units and that the mechanical coupling allowed by the lowering of symmetry is quite small. This behaviour is similar to the one observed in rare-earth molybdates [10]. In the compound investigated here the Mo–O stretching and bending vibration are shifted to lower wavenumbers compared to other compounds such as $Eu_2(MoO_4)_3$, $Sm_2(MoO_4)_3$, and $Gd_2(MoO_4)_3$ [10]. This may be explained by the pronounced distortion of the MoO_4 tetrahedra in the monoclinic polymorph of Tl_2MoO_4; three Mo–O distances are quite similar (1.7, 1.7, and 1.72 Å), yet one Mo–O distance is lengthened considerable (1.80 Å) at ambient pressure [4].

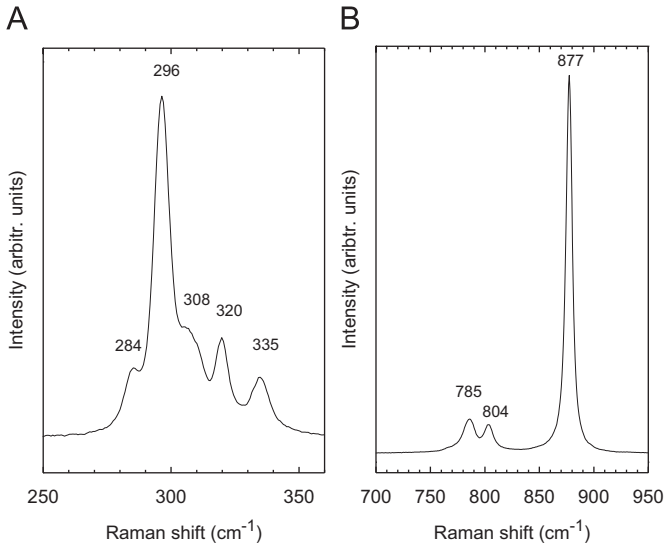

Fig. 1. Raman spectrum of Tl_2MoO_4 at ambient conditions. (A) Bending modes and (B) stretching modes of the MoO_4 tetrahedra.

3.1.1. Raman spectra in the pressure range 0.1–4.3 GPa

Fig. 2 shows the evolution of the Raman spectra with increasing pressure. The stretching modes and some of the bending modes upshift as expected under pressure. However, the two bending modes initially at 284 and 296 cm^{-1} shift to lower wavenumbers. This observation indicates that the pressure does not only induce a hardening of the modes but also a modification of the tetrahedral unit as evidenced by the X-ray diffraction as discussed in the next section.

The Raman spectra under high-pressure reflect the occurrence of a structural phase transition between 2.9 and 3.5 GPa, as in this pressure region the spectra show the appearance of new peaks (Fig. 2). The observed transition pressure is in good agreement with the one obtained from the X-ray diffraction data (see below). Additional peaks may be due to a further lowering of the symmetry, to an increase the number of formula units per primitive cell, and/or to an orientational disorder of the MoO_4 tetrahedra developing under pressure [11].

3.1.2. Raman spectra in the pressure range 4.3–9.5 GPa

At higher pressure, the behaviour is extremely dependent on the local hydrostaticity as often found in this A_2BX_4 family of compounds [11–13]. Two main pressure-induced evolutions can be distinguished depending on the location in the high-pressure cell (Figs. 3 and 4). This behaviour clearly indicates that the local conditions influence the transformation. In spot 1 (Figs. 3 and 4), we observed a transformation to an ordered phase. This phase probably undergoes a phase transition above 8.1 GPa. In spot 2, the spectra indicate an important degree of orientational disordering of the MoO_4 tetrahedra. This is evidenced by the fact that at least four bands associated with the v_1 vibration can be observed. In addition, the number of bending modes is also increased leading to a broad band. The relative intensity of the stretching modes in this spot is significantly lower than in spot 1. With increasing pressure the spectra in spot 2 become broader

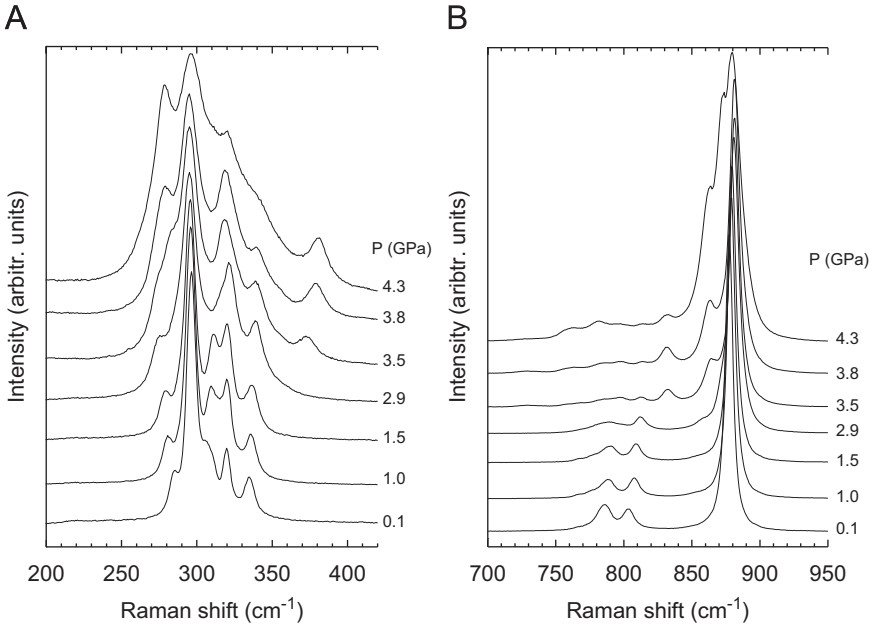

Fig. 2. Raman spectrum of Tl_2MoO_4 with increasing pressure. (A) Bending modes and (B) stretching modes of the MoO_4 tetrahedra.

and tend to resemble the spectra obtained on pressure-induced amorphous rare-earth molybdates [1]. Spectra at higher pressure were not recorded due to heating effect induced by the fact that our sample became black as discussed in the next section.

3.2. Optical absorption

The compression of the crystal is accompanied by a change in its colour (Fig. 5). At ambient pressure the crystals are light yellow, with increasing pressure the colour is changed to orange—red—dark red. The absorption edge decreases with increasing pressure in the spectral range available with our spectrometer with a slope of $dE/dP = -0.16(2)$ eV GPa^{-1}. This colour variation of the sample with pressure clearly indicates a change in the bandgap of Tl_2MoO_4.

We noticed that the rapid evolution of the optical absorption edge starts after the phase transition. Using our spectrometer, we could not measure the whole visible spectral range at each pressure but if we extrapolate the absorption edge at ambient pressure using Fig. 5, this edge is at 387 nm (3.2 eV) and is not in agreement with the yellowish colour of our starting material. On the other hand, if we calculate the optical absorption edge at the transition pressure $P_c = 3.2$ GPa, one finds a value of 466 nm (2.7 eV), in better agreement with the optical properties of our sample.

Therefore, there are strong indications that a change of the electronic structure is concomitant with the structural transformation. This may be due to some change of oxygen hybridization

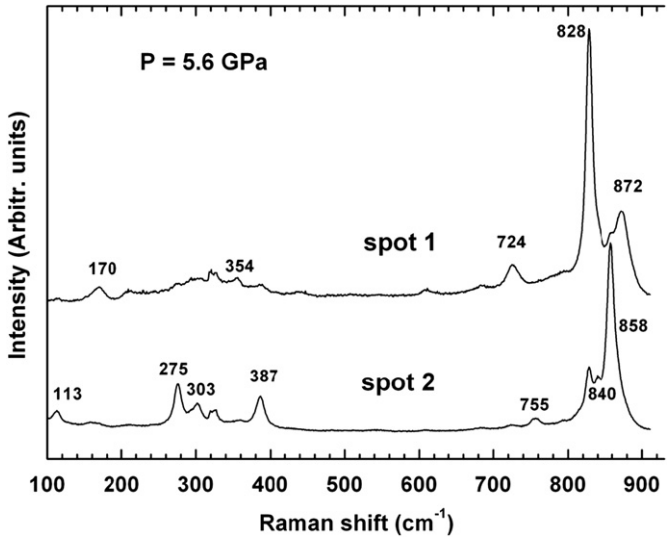

Fig. 3. Raman spectra of Tl_2MoO_4 at 5.6 GPa in two different spots of the sample chamber inside the diamond anvil cell.

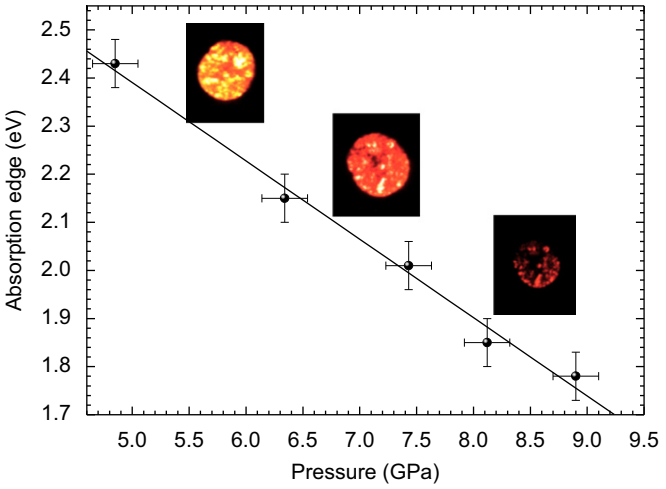

Fig. 5. Optical absorption of Tl_2MoO_4 as a function of pressure. The slope of the fitted line to the experimental data is $dE/dP = -0.16(2)$ eV GPa^{-1}.

Table 2
Lattice parameters and unit-cell volumes as a function of pressure.

Pressure (GPa)	a (Å)	b (Å)	c (Å)	β (deg.)	V (Å^3)
0.0001	10.565(3)	6.418(1)	8.039(2)	91.05(4)	545.0(3)
0.90	10.424(2)	6.362(1)	7.959(6)	91.29(4)	527.7(4)
1.76	10.305(2)	6.310(1)	7.880(6)	91.61(4)	512.2(4)
2.40	10.237(2)	6.269(1)	7.806(4)	91.82(4)	500.7(3)
3.20	10.173(2)	6.220(1)	7.764(5)	91.97(4)	491.0(3)

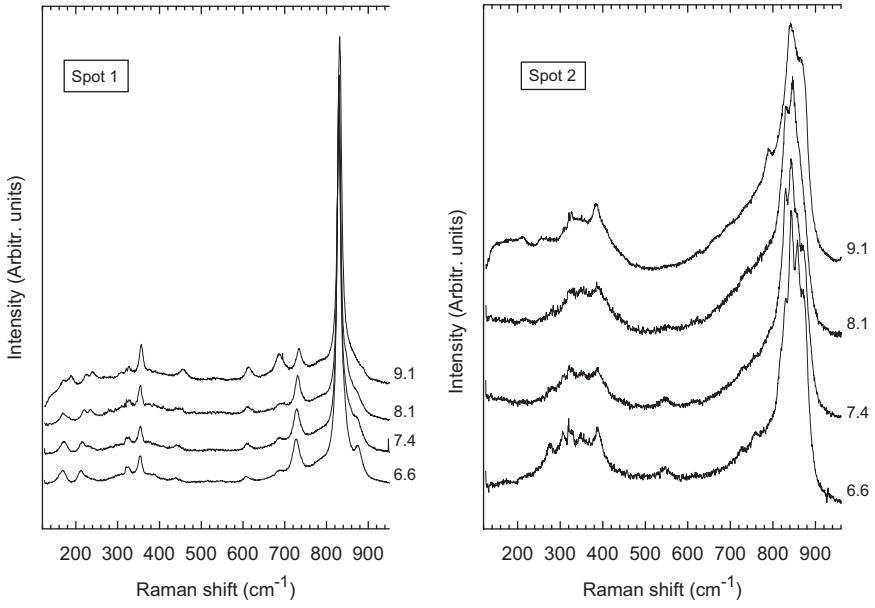

Fig. 4. Evolution of the Raman spectra of Tl_2MoO_4 at high pressure in two different zones of the sample chamber inside the diamond anvil cell.

accompanying the MoO_4 tetrahedron interaction evidenced in the following part.

3.3. X-ray diffraction

A series of X-ray measurements was performed up to pressures of 7.33 GPa. The acentric, monoclinic polymorph was only stable to 3.20 GPa. At higher pressures, no single-crystal reflections were detected any more. Instead, weak and strongly smeared incomplete Debye–Scherrer rings were visible in the diffraction diagrams on the image plate. These observations indicate that the thallium molybdate undergoes a first-order pressure-induced phase transition above 3.20 GPa, which leads to the destruction of the single crystal.

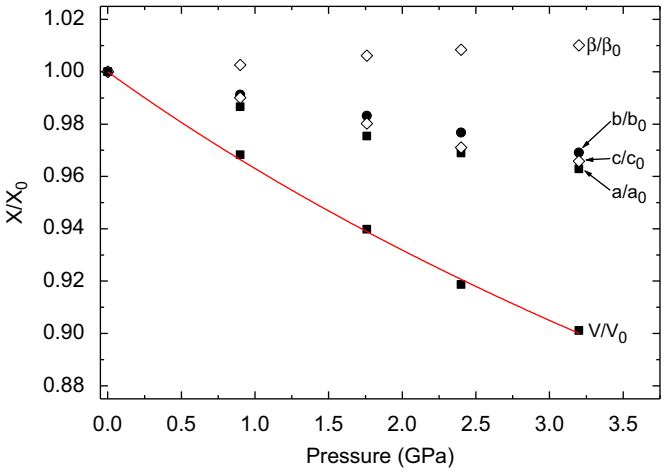

Fig. 6. Pressure dependence of normalized lattice parameters and unit cell volumes, $a_0=10.565(3)$ Å, $b_0=6.418(1)$ Å, $c_0=8.039(2)$ Å, $\beta_0=91.05(4)^\circ$, and $V_0=545.0(3)$ Å^3. The line is the EoS fit to the bulk compressibility data.

Table 3
Experimental X-ray data for the single-crystal measurement at 3.20 GPa.

Crystal data	
Space group	*C*2 (No. 5)
Z	4
a (Å)	10.173(2)
b (Å)	6.220(1)
c (Å)	7.764(5)
β (deg.)	91.97(4)
V (Å^3)	491.0(3)
ρ (g/cm^3)	7.6126
μ (mm^{-1})	67.197
Data collection	
No. of measured refl.	1865
Range of *hkl*	$-12 \le h \le 12$ $-7 \le k \le 7$ $-3 \le l \le 3$
No. of unique refl.	900
No. of observed refl. [a]	208
$R(\text{int})_{\text{obs/all}}$ [b]	5.18/6.37
$\sin(\theta)/\lambda$	0.661759
Refinement [b]	
R_{obs}	3.69
wR_{obs}	2.99
R_{all}	9.02
wR_{all}	3.41
GoF_{all}	1.29
GoF_{obs}	1.07
No. of parameters	25

[a] Criterion for observed reflections is $|F_{\text{obs}}| > 3\sigma$.
[b] All agreement factors are given in %, weighting scheme $1/[\sigma^2(F_{\text{obs}})+(0.01F_{\text{obs}})^2]$.

The lattice parameters up to 3.20 GPa are shown in Table 2 and Fig. 6. In this pressure range, the axial compressibilities are quite similar. On the other hand, the monoclinic *β* angle slightly increases. The bulk compressibility *P*–*V* data could be fitted by a Birch–Murnaghan equation of state with the zero-pressure bulk modulus $B_0=24.6(4)$ GPa and the unit-cell volume at ambient pressure $V_0=545.1(5)$ Å^3 for the first pressure derivative of the bulk modulus $B'=4.0$.

The results of our structural refinement of the data measured at 3.20 GPa using the coordinates from the ambient-pressure model as starting coordinates [4] are given in Tables 3–5. The displacement parameters for all the atoms were treated isotropically. In addition, the parameters for all the O atoms were restricted to be equal. A test for additional twinning, taking into account both the threefold axis (lost in the temperature-induced transition $P\bar{3}m1 \rightarrow C2$) and the inversion center as twinning operations, showed the investigated crystal to be unaffected by twinning.

Fig. 7 shows the crystal structure of Tl_2MoO_4 (*C*2, *Z*=4) at 3.20 GPa, just below the phase transition. The most important

Table 4
Positional and isotropic thermal displacement parameters (in Å^2) at 3.20 GPa.

Atom	*x*	*y*	*z*	U_{iso}
Tl1	0.0	0.0	0.0	0.030(1)
Tl2	0.0	0.0742(6)	0.5	0.021(1)
Tl3	0.3327(3)	0.0260(11)	0.1682(11)	0.031(1)
Mo	0.6636(6)	0.0251(24)	0.3152(22)	0.032(2)
O1	0.718(3)	−0.064(5)	0.526(7)	0.049(6)
O2	0.550(3)	0.244(5)	0.293(11)	0.049(6)
O3	0.809(3)	0.096(5)	0.200(10)	0.049(6)
O4	0.589(4)	−0.179(6)	0.211(11)	0.049(6)

Table 5
Selected interatomic distances (Å) and angles (deg.) at 3.20 GPa.

Distances (Å)		
Tl1–O3	(2x)	2.60(5)
Tl1–O4	(2x)	2.73(6)
Tl1–O2	(2x)	2.83(7)
Tl2–O2	(2x)	2.68(6)
Tl2–O4	(2x)	2.90(7)
Tl2–O3	(2x)	3.00(6)
Tl2–O1	(2x)	3.01(4)
Tl2–O1	(2x)	3.17(3)
Tl3-O1		2.52(5)
Tl3–O3		2.71(3)
Tl3–O2		2.75(4)
Tl3–O4		2.92(4)
Tl3–O4		3.12(4)
Tl3–O3		3.20(7)
Tl3–O4		3.35(8)
Tl3–O2		3.54(4)
Tl3–O3		3.58(3)
Mo–O4		1.68(5)
Mo–O2		1.79(4)
Mo–O1		1.80(5)
Mo–O3		1.81(5)
Mo–O1		3.08(4)
Angles (deg.)		
O1–Mo–O2		120(3)
O1–Mo–O3		107(2)
O1–Mo–O4		109(3)
O2–Mo–O3		107(2)
O2–Mo–O4		105(2)
O3–Mo–O4		108(3)

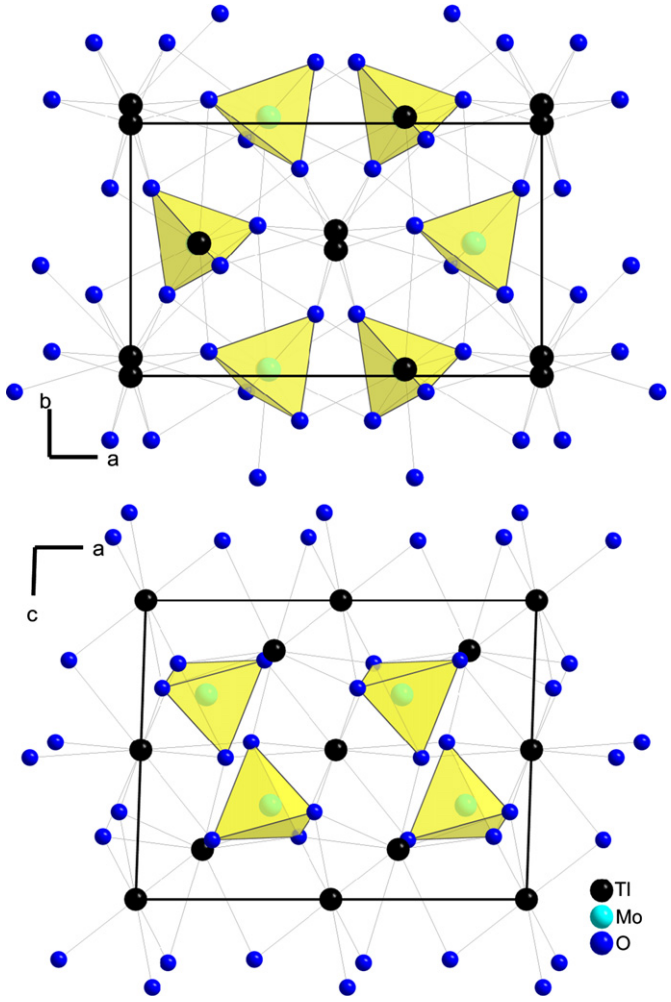

Fig. 7. Crystal structure at 3.20 GPa. The tetrahedra around the Mo atoms are drawn.

change in the structure when compared to the ambient pressure structure concerns the neighbourhood of the Mo-ion. Although, the first coordination sphere of Mo is still formed by four oxygen atoms, three of the Mo–O distances (Mo–O1, Mo–O2, Mo–O3) are significantly increased under pressure and only one of the distances shrinks (Mo–O4). A comparison of the **B**ond **V**alence **S**ums calculated according to Ref. [14] shows that the value for Mo is decreased from 6.4 v.u. at ambient pressure to 5.85 v.u. at 3.20 GPa. In addition, the distance to the next nearest oxygen atom, which is 3.44 Å in the ambient pressure phase [4], is now drastically shortened to a value of 3.08 Å. At the same time one of the tetrahedral angles is significantly increased (O1–Mo–O2: 114.5(7)° at ambient pressure as compared to 120(3)° at 3.20 GPa). The coordination around Mo thus tends to increase at higher pressures. This high-pressure behaviour is similar to the results of simulation obtained on rare-earths molybdates [1,15]. If one takes into account this additional Mo–O distance, a condensation of the MoO_4-tetrahedra into corner connected chains of MoO_5-polyhedra running parallel to the crystallographic *b*-axis is achieved (Fig. 8) under pressure. Assuming that this Mo–O distance would be further shortened at higher pressures, the anticipated coordination change around Mo, together with the strong "underbonding" is probably closely related to the phase transition, which leads to the destruction of the crystal. This increased Mo coordination at the phase transition is consistent

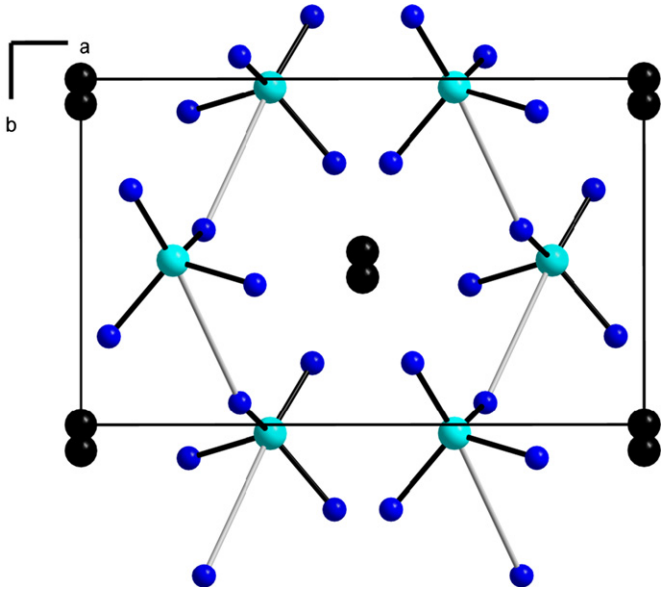

Fig. 8. Crystal structure at 3.20 GPa showing the chains of the corner-sharing MoO_5 polyhedra. The tetrahedral Mo–O distances below 1.81 Å are drawn thick black, while the Mo–O distance of 3.08 Å is drawn as thick light gray (see Table 5).

with Raman spectroscopy results with a clear downshift of the vibrational modes in the high-pressure phase.

There are no pressure-induced changes of the coordination numbers for the Tl1, Tl2, and Tl3 atoms and the connection pattern between tetrahedral units and Tl–O polyhedra is also not substantially changed with increasing pressure. As a general trend one observes a shortening of the Tl–O distances with increasing pressure and polyhedral volumes of the TlO-polyhedra are decreased by 12% ($Tl1O_6$ and $Tl2O_{10}$) and 10% ($Tl3O_9$) at 3.20 GPa when compared to the volumes at ambient pressure. A good measure for the stereochemical activity of the lone pair is the eccentricity of the corresponding polyhedra. Calculations carried out with the program IVTON [16] show a decrease of eccentricity for the $Tl1O_6$ and $Tl3O_9$ polyhedra with increasing pressure, indicating decreasing stereoactivity for the corresponding lone pairs. For the $Tl2O_{10}$-polyhedra, on the other hand, the eccentricity increases i.e., the stereoactivity is more pronounced in the high pressure phase. This behaviour is different from the one observed for Tl_2SeO_4 (a compound which also has isolated tetrahedral building units [17]), where the lone-pair electrons of the two symmetrically independent Tl^+ ions show a decrease of stereochemical activity with increasing pressure, although in a different degree for both sites. Similar behaviour of the stereoactivity of the lone electron pairs was also observed for Tl_2CO_3 [18,19], which like Tl_2MoO_4 loses its crystallinity at high pressures (>5.82 GPa).

4. Conclusions

Both Raman spectroscopy and single crystal X-ray diffraction show that the monoclinic polymorph of Tl_2MoO_4 is stable up to 3.20 GPa. At $P_c = 3.5 \pm 0.5$ GPa, a structural first-order phase transition is observed leading to the destruction of the studied single crystal. At a pressure just below the transition, the volume of the MoO_4 tetrahedra is considerably increased when compared to ambient pressure, leading to a strong "underbonding" of the Mo-ion. Depending on the local hydrostatic conditions, the high-pressure phase may be more or less ordered. A strong orientational disordering can develop and one may expect that the ultimate step of this process would result in an amorphous compound.

This effect is similar in rare-earths molybdates as demonstrated by ab initio calculations and X-ray absorption experiments. It is remarkable that in compounds structurally and chemically different but with MoO_4 as basic units, a general trend under pressure can be observed. These pressure-induced effects are most probably the underlying reason for the structural phase transition. In addition, we showed that the stereoactivity of the lone-pair electrons on the three symmetrically independent Tl-sites is not uniform; while for two sites the stereoactivity decreases with increasing pressures for the third site the stereoactivity increases.

Acknowledgments

KF and AG acknowledge financial and technical support from the Spanish Ministerio de Ciencia e Innovación (Grant no. FIS2008-03834), the Gobierno Vasco, and SGIker (UPV/EHU).

References

[1] O. LeBacq, D. Machon, D. Testemale, A. Pasturel, submitted for publication.
[2] M. Gaultier, G. Pannetier, Rev. Chim. Miner. 9 (1972) 271–289.
[3] K. Friese, G. Madariaga, T. Breczewski, Acta Crystallogr. C 55 (1999) 1753–1755.
[4] K. Friese, M.I. Aroyo, C.L. Folcia, G. Madariaga, T. Breczewski, Acta Crystallogr. B 57 (2001) 142–150.
[5] (a) H. Ahsbahs, Z. Kristallogr. (Suppl. 9) (1995) 42;
(b) H. Ahsbahs, Z. Kristallogr. 219 (2004) 305–308.
[6] X-AREA: Stoe IPDS Software. Stoe & Cie GmbH, Darmstadt, Germany.
[7] (a) G.J. Piermarini, S. Block, J.D. Barnett, R.A. Forman, J. Appl. Phys. 46 (1975) 2774–2780;
(b) H.K. Mao, J. Xu, P.M. Bell, J. Geophys. Res. 91 (1986) 4673–4676.
[8] V. Petricek, M. Dusek, L. Palatinus, Jana 2006. The crystallographic computing system. Institute of Physics, Praha, Czech Republic.
[9] K. Nakamoto, in: Infrared and Raman Spectra of Inorganic and Complex Compounds, 5th edition, Wiley-Interscience, New York, 1997.
[10] G. Lucazeau, D. Machon, J. Raman Spectrosc. 37 (2006) 189–201.
[11] D. Machon, A. Grzechnik, K. Friese, J. Phys.: Condens. Matter 21 (2009) 405405.1–405405.11.
[12] D. Machon, V.P. Dmitriev, P. Bouvier, P.N. Timonin, V. Shirokov, H.-P. Weber, Phys. Rev. B 68 (2003) 144104.1–144104.7.
[13] D. Machon, P. Bouvier, H.-P. Weber, P. Tolédano, J. Phys.: Condens. Matter 18 (2006) 3443–3453.
[14] N.E. Brese, M. O'Keeffe, Acta Crystallogr. B 47 (1991) 192–197.
[15] G. Lucazeau, P. Bouvier, A. Pasturel, O. Le Bacq, T. Pagnier, Acta Phys. Pol. 116 (2008) 25–31.
[16] T. Balic-Zunic, I. Vickovic, J. Appl. Cryst. 29 (1996) 305–306.
[17] A. Grzechnik, T. Breczewski, K. Friese, J. Solid State Chem. 181 (2008) 2914–2917.
[18] A. Grzechnik, K. Friese, Acta Crystallogr. C 64 (2008) i69–i70.
[19] A. Grzechnik, K. Friese, Acta Crystallogr. C 66 (2010) i37–i38.